Indian Journal of Biochemistry & Biophysics
Vol. 62, October 2025, pp. 1129-1141
DOI: 10.56042/ijbb.v62i10.17233

Computational analysis of *N*2-Aryl-1,2,3-triazoles as potential multi-target inhibitors

Sunkara Muni Sireesha[1, 2], and Beda Durga Prasad[1]*

[1]Department of Pharmaceutical Chemistry, GITAM School of Pharmacy, GITAM (Deemed to be) University, Hyderabad-502 329, Telangana, India

[2]Department of Pharmaceutical Chemistry, Sarojini Naidu Vanita Pharmacy Maha Vidyalaya, Hyderabad-500 017, Telangana, India

Received 18 February 2025; *revised 03 July 2025*

Triazole derivatives, synthesized using green chemistry, are promising therapeutics due to their strong pharmacokinetics, pharmacodynamics, and ADMET properties. Their proven activities against various conditions have increased industrial demand. Notably, *N*2-Aryl-1,2,3-triazoles contain heterocyclic nitrogen structures, making them a valuable platform for new drug development. We evaluated 173 *N*2-Aryl-1,2,3-triazoles obtained from the PubChem database, assessed their ADMET properties,and optimized their structures using the Universal Force Field (UFF). *In silico* assessments of pharmacological properties were performed. Four key target proteins were identified: HDAC8 (antidiabetic), APC (anticancer), and CYP51 (antitubercular/antibacterial and antifungal), with docking studies conducted on each target.Top hits included CID-135064814 (-8.8 kcal/mol, antidiabetic/anticancer), CID-59814079 (-9.6 kcal/mol, anticancer), CID-139251519 (-10.6 kcal/mol, antibacterial/antitubercular), and CID-102473643 (-13.8 kcal/mol, antifungal), demonstrating the highest binding affinities. Other notable best docked molecules were CID-135064814, CID-102473643, and CID-135066341. CID-135065731, CID-59814079, CID-21331374, CID-88817443, CID-59814075, CID-54036863, and CID-70598857.We conducted human proteome target analysis for the best-docked molecules. A 100 ns molecular dynamics simulation for the overall best-docked compound was done. We successfully screened the molecules that showed the best results and that had multitarget capability.

Keywords: *Adenomatous polyposis* coli, Cytochrome P450, Docking, Drug designing, Histone deacetylase 8, *N*2-Aryl-1,2,3-triazoles, Virtual screening

Triazoles are synthetic molecules with nitrogen-containing heterocyclic ring structures. These molecules are bioisosteres and may have multiple derivatives with similar physicochemical properties and bioactivities, and these molecules are not naturally available. The structural components and functional groups are replaceable through various established reactions, such as aryl halides, alkynes, and others. Substitution of the N2 group and arylation was successfully reported in many studies, including the achievement of N2-selective arylation of 4,5-unsubstituted or 4-substituted 1,2,3-triazoles[1]. Other regioselective synthesis methods, such as electrooxidation coupling, were successfully used to synthesize *N*2-Aryl-1,2,3-triazoles[2] and from diaryliodonium salts[3]. Photoluminescent metal-organic frameworks (MOFs) were also developed using these triazole compounds for biomolecule sensing[4].

Several synthetic compounds are approved for their therapeutic potential by regulatory agencies globally for various health conditions. However, the continuous development of novel, effective therapeutic molecules is challenging and requires innovative approaches. Heterocyclic nitrogen-containing molecules are used for multiple purposes, including very effective therapeutics. Triazoles and the associated derivatives garnered special attention due to their bioisosteres properties and high level of bioactive nature. The pharmacokinetic and pharmacodynamic properties of the compound series belonging to the triazole, thiadiazole, thiazole, oxadiazole, and other azole derivatives are impressive and are being used as therapeutic platforms for antidiabetic, anticancer, antimicrobial, anti-inflammatory, antitubercular, and antiviral treatments. Individual studies have reported the effectiveness of these compounds against specific molecular targets or pathogenic conditions. Due to the effective implementation of a green chemistry-based synthesis

*Correspondence:
E-mail: dbeda@gitam.edu

approach, the development of new compounds has accelerated in recent years. However, the evaluation of the therapeutic potential and pharmacological efficacy of this large number of compounds for different targets is a challenging task.

Computer-aided drug design (CADD) aided the acceleration of small-molecule screening. Many studies have reported successful implementation of CADD, including homology modeling, docking, quantitative structure-activity relationship (QSAR), and molecular dynamics (MD) simulation techniques in screening and understanding the important target proteins and the best possible interacting ligand molecules[5]. A combination of experimental and modern computational drug-designing approaches has been used to target perilous pathogens such as Mycobacterium[6], and other alarming diseases like diabetes[7].

All these computational approaches, along with synthesis and biological activity evaluation, were attempted with triazole molecules, including *N*2-Aryl-1,2,3-triazoles earlier[8]. However, limited studies attempted to understand the therapeutic potential of *N*2-Aryl-1,2,3-triazoles for multiple drug targets simultaneously. In the present study, we attempted to understand the potential binding affinities of the *N*2-Aryl-1,2,3-triazoles molecules (n=173) for four different targets, namely antidiabetic, anticancer, antitubercular, and antifungal simultaneously. The study objective was to identify the most effective *N*2-Aryl-1,2,3-triazole compounds that could be used for multiple targets simultaneously using a computational approach.

Materials and Methods

A computational screening approach was adopted to select the small molecules and target them for specific proteins that may be effective for developing potential therapeutics for diabetes, cancer, tuberculosis, and fungal infections.

Molecule selection and database

*N*2-Aryl-1,2,3-triazole molecules were collected from the PubChem database. Molecules that were >85% structurally similar were selected, and the Lipinski filter was used to screen the molecules. SMILE (Simplified Molecular Input Line Entry System) notations for each molecule were collected from the database. A database of the identified molecules was created, and possible duplicate entries were removed to ensure the accuracy of the data collection. OpenBabel was used for the structure format conversion[9].

Molecular mechanical optimization and ADME calculations

All the collected molecules (n=173) were subjected to energy minimization using Universal Force Field (UFF). RDKit libraries[10] were used for molecule minimization. All the collected and minimized molecules were used for *in silico* pharmacokinetic and pharmacodynamic characterization through the ADME (Absorption, Distribution, Metabolism, and Excretion) properties evaluation using SwissADME[11].

Target protein identification and docking

To assess binding affinity, target proteins were identified for diabetes/cancer, bacterial/tubercular, and fungal inhibitions after carefully reviewing the literature. For an antidiabetic study, HDAC8 (Histone Deacetylase 8) from a human source (PDB ID: 1T69) was selected. Similarly, to evaluate the anticancer inhibition activity, another human protein, APC (*Adenomatous Polyposis* Coli) (PDB ID: 3NMX), was selected. Mycobacterium cytochrome P450 (CYP51) (PDB ID: 1EA1) was chosen to understand the antibacterial inhibition of the selected molecules. The antifungal target protein selected was lanosterol 14α-demethylase (LDM), a (Cytochrome P450 51 (CYP51) from *Candida glabrata* (PDB ID:5JLC). The active sites were evaluated using the PrankWeb server (https://prankweb.cz/). AutoDock Vina was used for docking analysis[12], and visualization and analysis of the docking results were done using the Discovery Studio[13].

Molecular dynamics simulation

A 100 ns molecular dynamics (MD) simulation was done to evaluate the binding effectiveness of the best ligand to the target protein. The CHARMM36 force field[14] was used in the GROMACS 2022.4 software package[15] to run MD simulations on the protein-ligand complex. The Cgenff server[16] was utilized to generate the topologies and parameter files for the ligand. Additionally, the Particle Mesh Ewald (PME) method[17]was employed for the computation of electrostatic forces. The solvation of each ligand-protein pair was conducted with the transferable intermolecular potential with a three-point (TIP3P) water model[18]. The complex was put inside a dodecahedron-shaped box, with a buffer distance of 1 Å. The system's neutrality was attained by integrating Na+ and Cl- ions. The methodology of energy reduction, along with 5,000 iterations of the steepest descent method, effectively eased unfavorable connections and collisions within the protein

structure. The LINCS approach[19] was utilized to eliminate all hydrogen bonds, after which the total system was heated to a temperature of 310 K. Following energy minimization, the complexes experienced two consecutive equilibration phases. The preliminary stage consisted of a 1 ns equilibration in the NVT ensemble, succeeded by an additional 1 ns equilibration in the NPT ensemble. The velocity-rescaling method[20] was utilized for temperature coupling, while the Parrinello-Rahman technique[21] was applied to sustain constant pressure. A system that had attained equilibrium was utilized during the 100 ns production run. A thorough investigation of the entire system was performed utilizing the many analytical modules offered by the GROMACS program, concentrating on structural and conformational elements. The post-MD study encompassed RMSD, RMSF, SASA, and binding free energy.

Results

Small molecule collection and optimization

All the molecules in this study were collected from the PubChem database using the Lipinski filters mentioned in the method section. A total of 173 molecules were collected in .sdf format. Each molecule was optimized using the options mentioned in the method section. A difference in the optimized energy was observed, which ranged between 31.96 kcal/mol (CID-68559467) and 358.44 kcal/mol (CID-135065731).

ADMET properties evaluation

Structure characterization of the ligands

A total of 46 ADMET properties were calculated for all the molecules. The molecular weight of the molecules ranged between 251.33 g/mol (C16H17N3) and 505.63g/mol (C30H22KN6). The molar mass values of these small molecules were between 73.74 grams/mole and 145.5 grams/mole. The number of heavy atoms ranged between 17 and 37 in these selected molecules. Similarly, the aromatic heavy atoms ranged between 11 and 35. The sp3-bonded carbon atom percentage ranged between 0 and 0.6. The number of rotatable bonds, hydrogen bond acceptors, and hydrogen bond donors ranged between 3-12, 2-7, and 0-2, respectively. The topological polar surface area (TPSA) of these selected molecules was between 25.78 Å^2 and 135.07 Å^2. Along with various logP parameters such as implicit log (iLOGP), XLOGP3, and water partition coefficient (WlogP), GI absorption level, blood-brain-barrier (BBB) permeability, and various Cytochrome P-450 (CYP; CYP1A2, CYP2C19, CYP2C9, CYP2D6, and CYP3A4) inhibitor activity of the molecules were predicted (Fig. 1). The estimated bioavailability for the molecules was ≥0.55, which was ideal for GI absorption. The GI absorption level and BBB permeability observed were high, with most of the molecules being Pgp substrates with predicted varying CYP inhibition activity (Fig. 1).

Target protein collection and optimization

The triazole molecules have known inhibitory activity for many types of target proteins that include antibacterial[22], antifungal[23-24], antidiabetic[25-26], and anticancer[27-28]. Also, several reports mentioned that triazoles are excellent antitubercular agents[29-30]. However, most of the studies focused on a specific activity of various triazole molecules. In the present study, we wanted to compare the possible inhibitory activity of the selected compounds against important proteins of all these target types.

Histone Deacetylase (HDAC) proteins are an important group of proteins known to promote insulin resistance.Most of the class I HDACs, including HDAC8, can promote insulin resistance. Specifically, HDAC1 can inhibit glucose transport and impair GLUT4 function[31]. We have selected the human HDAC8 protein (PDBID: 1T69), an important therapeutic target[32-33], to evaluate the potential inhibitory activity of the selected molecules. The role of *Adenomatous Polyposis* coli (APC) protein in tumor suppression is well documented[34-35]. The

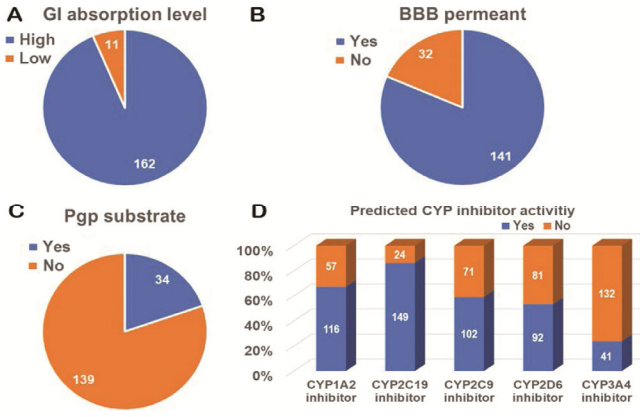

Fig. 1 — Predicted ADMET analyses of the selected molecules (n=173). (A) Comparative GI absorption level of the molecules; (B) Comparative blood-brain barrier (BBB) permeability of the molecules; (C) Prediction results of the P glycoprotein (Pgp) substrate evaluation; and (D) Predicted various Cytochrome P-450 (CYP; CYP1A2, CYP2C19, CYP2C9, CYP2D6, and CYP3A4) inhibitor activity of the molecules

human APC protein (PDBID: 3NMX)[36] was chosen as the potential anticancer target for the molecules. We have chosen Mycobacterium CYP51 protein (PDB ID: 1EA1)[37] as an antibacterial/antitubercular target. For the antifungal target, the CYP51 protein from *Candida glabrata* (PDB ID: 5JLC)[38] was selected.

Active site identification

PrankWeb[39] was used to evaluate and understand the microenvironment of the target pockets.

Molecular docking

All selected and optimized compounds (n=173) were docked in the considered four targets (Suppl 1) (antidiabetic, anticancer, antibacterial, and antifungal). The best docked binding energy values are represented in (Table 1) for each target.

Docking against antidiabetic and anticancerHDAC8 target

The HDAC proteins play a crucial role in gene expression regulation and are also directly involved in shaping the chromosomal structure[31]. These proteins are segregated into four different classes, class I through class IV. The class I HDACs include HDAC1, HDAC2, HDAC3, and HDAC8. In this study, human HDAC8 (PDB ID: 1T69) is the target protein. This target protein can be considered an anticancer target as well, and HDAC8 plays a vital epigenetic regulatory role for the important transcription factors essential for tumorigenesis[32].

The docking exercise outcomes for the selected molecules (n=173) suggested CID-135064814 (binding energy -8.8 kcal/mol) (Fig. 2A & B), and CID-102473643 (binding energy -8.4 kcal/mol) are the best molecules. The molecular interaction analysis suggested Pi-Pi stacked and shaped bond formation by the Phe152 and Phe207 with the benzene ring structures of the compound (CID-135064814) (Fig. 2C).

The Phe208 residue formed a bond with the benzene ring through a π-donor hydrogen bonding

Table 1 — Best docking results obtained against the antidiabetic, anticancer, antibacterial, and antifungal target proteins

Category	Protein type	PDB ID	Ligand ID	Binding Energy (kcal/mol)	Structure	Interacting residues
Antidiabetic/Anticancer	Human HDAC8	1T69	CID-135064814	-8.8	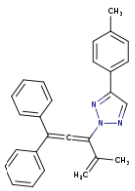	Tyr100, Tyr306, Met274, Phe152, Phe207, Phe208
			CID-102473643	-8.4	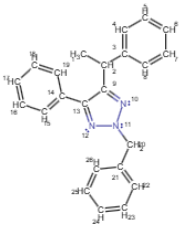	Tyr306, met274, phe207, phe208, phe152, lys33, gly206, asp101, His143, His180
Anticancer	Human APC	3NMX	CID-59814079	-9.6	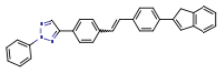	His408, Asn627, Gln412, Thr626, Asp539
			CID-21331374	-9.4	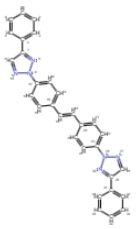	Gln412, Pro448, Ala449, Asn188, Gln542, Leu190, Val452, Ile191, Ser192, Lys455, His408, Asn627

(*Contd.*)

Table 1 — Best docking results obtained against the antidiabetic, anticancer, antibacterial, and antifungal target proteins (*Contd.*)

Category	Protein type	PDB ID	Ligand ID	Binding Energy (kcal/mol)	Structure	Interacting residues
Antibacterial	Mycobacterium CYP51 (Cytochrome P450)	1EA1	CID-139251519	-10.6	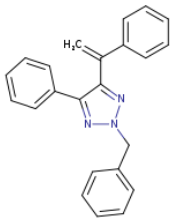	Thr260, Leu321, Ala256, Leu100, Arg96, Tyr76
			CID-101187610	-10.5	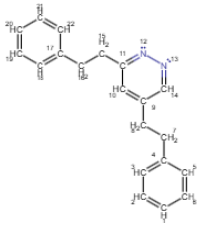	Phe78, Val434, Leu321, Ala256, Leu100, Gln72, Arg96
Antifungal	Candida glabrata CYP51	5JLC	CID-59814079	-13.8	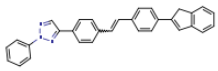	Ile140, Tyr141, Phe242, Leu381, Met512, His382, Tyr73
			CID-59814075	-13.7	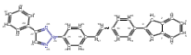	Leu96, Tyr73, Ile140, Tyr141, Met512, Phe242, Leu81

(Fig. 2C). Met274 showed a bond formation with the help of sulfur. However, the Tyr100 andTyr306 formed bonds with the carbon molecules outside the benzene ring structure of the ligand. Almost similar interactions were observed for the other ligand (CID-102473643), resulting in a higher binding energy (-8.4 kcal/mol) (Table 1).

Docking against anticancer APC target

The APC protein has an important role in tumor suppression, where it has a cascading effect in Wnt/β-catenin signaling, and this protein acts as an apoptosisand differentiation inducer, supporting impaired cellular proliferation, and is a tumor suppressor[34-35]. This protein is an anticancer molecular target, especially in colorectal cancer, and has several therapeutic implications. We have docked the selected molecules (n=173) in the pocket of the selected target human APC protein (PDB ID:3NMX), and the obtained best ligand (CID-59814079; binding energy -9.6 kcal/mol) was analyzed specific interactions (Fig. 3A & B). The type of bond formation observed were donor-donor interactions with His408, Asn627, and Gln412 residues, Pi interaction with Asp539, and Fi-sigma interaction with Thr626 (Fig. 3C). Another compound with high binding affinity was CID-21331374 (9.4 kcal/mol) (Table 1).

Docking against mycobacterium cytochrome P450 target

To understand the binding affinity of the selected 1,2,3triazole compounds against the bacterial or specifically mycobacterium target, cytochrome P450 (CYP51) from Mycobacterium (PDB ID:1EA1) was considered as the target protein. The best ligand obtained with a binding energy of -10.6 kcal/mol was compound CID-139251519 (Fig. 4A & B), and CID-101187610 (-10.5 kcal/mol) (Table 1). Pi-Pi and Pi-sigma interactions were observed for Thr260, Leu321, Ala256, Leu100, and Tyr76 (Fig. 4C)with various

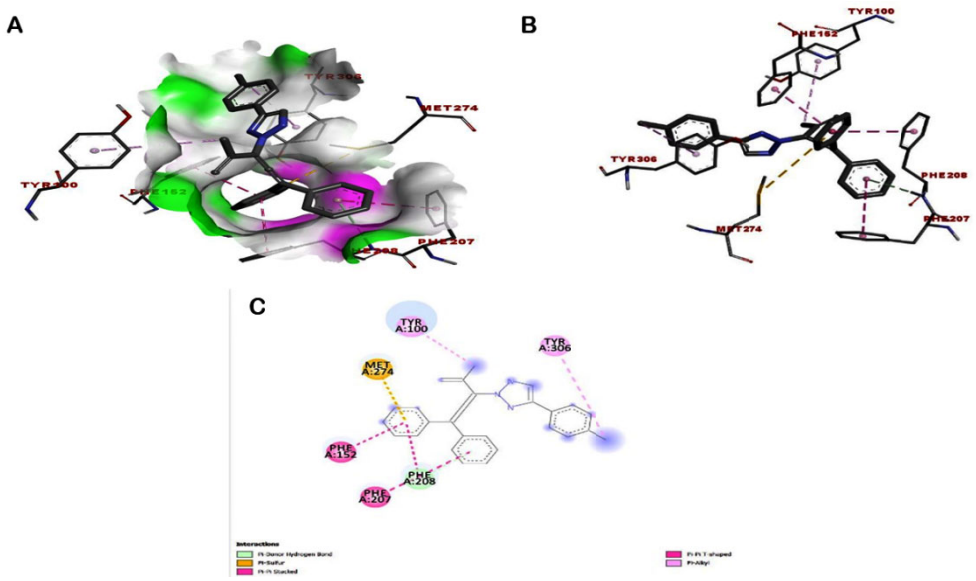

Fig. 2 —Docking results against the antidiabetic/anticancer HDAC8 protein (PDB ID: 1T69) for CID-135064814 with binding energy -8.8 kcal/mol. (A) The ligand molecule (black stick) was docked inside the binding pocket of the target protein. Protein residues around the ligand are shown as sticks with residue names and sequence numbers labeled in red. A molecular surface (semi-transparent white/gray) indicates the protein's surface around the ligand. Color shading (green and magenta), highlighting specific surface properties or interaction regions, where green color represents the hydrophobic regions, and the magenta indicates the aromatic or π–π interaction areas. The dashed lines show potential interactions (*e.g.*, hydrogen bonds, π–π stacking, *etc.*); (B) The amino acid residues of the target protein are specifically labeled with residue names, chain identifiers, and positions; and (C) The most important interactions between the ligand and the target protein are shown. The types of interactions are shown in different color codes on the left and right sides

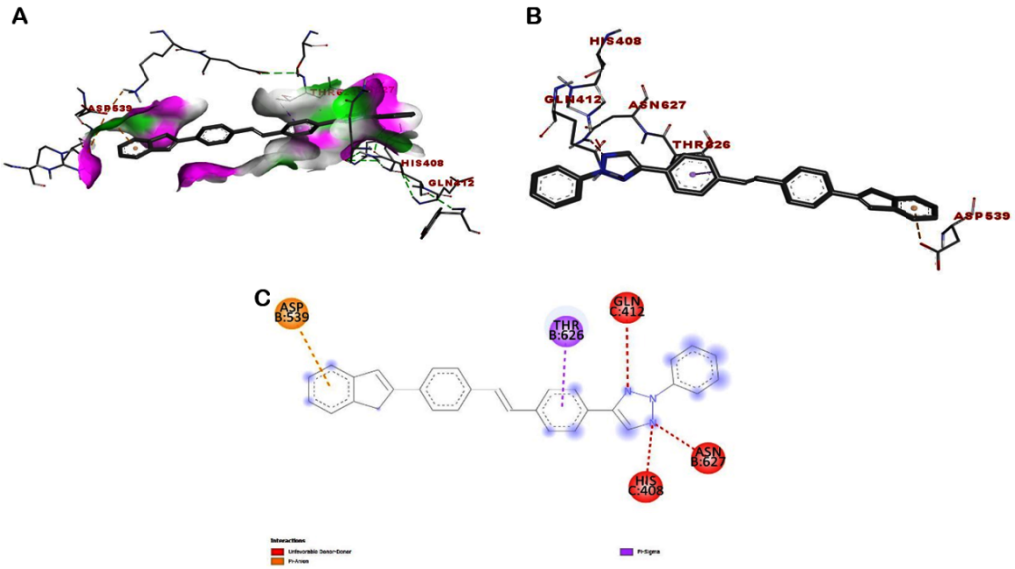

Fig. 3 — Docking results for the anticancer target human APC protein (PDB ID: 3NMX). Presentation of the best ligand (CID-59814079) protein interactions (binding energy -9.6 kcal/mol) observed. (A) The ligand molecule (black stick) was docked inside the binding pocket of the target protein. Protein residues around the ligand are shown as sticks with residue names and sequence numbers labeled in red. A molecular surface (semi-transparent white/gray) indicates the protein's surface around the ligand. Color shading (green and magenta), highlighting specific surface properties or interaction regions, where green color represents the hydrophobic regions, and the magenta indicates the aromatic or π–π interaction areas. The dashed lines show potential interactions (*e.g.*, hydrogen bonds, π–π stacking, *etc.*); (B) The amino acid residues of the target protein are specifically labeled with residue names, chain identifiers, and positions; and (C) The most important interactions between the ligand and the target protein are shown. The types of interactions are shown in different color codes on the left and right sides

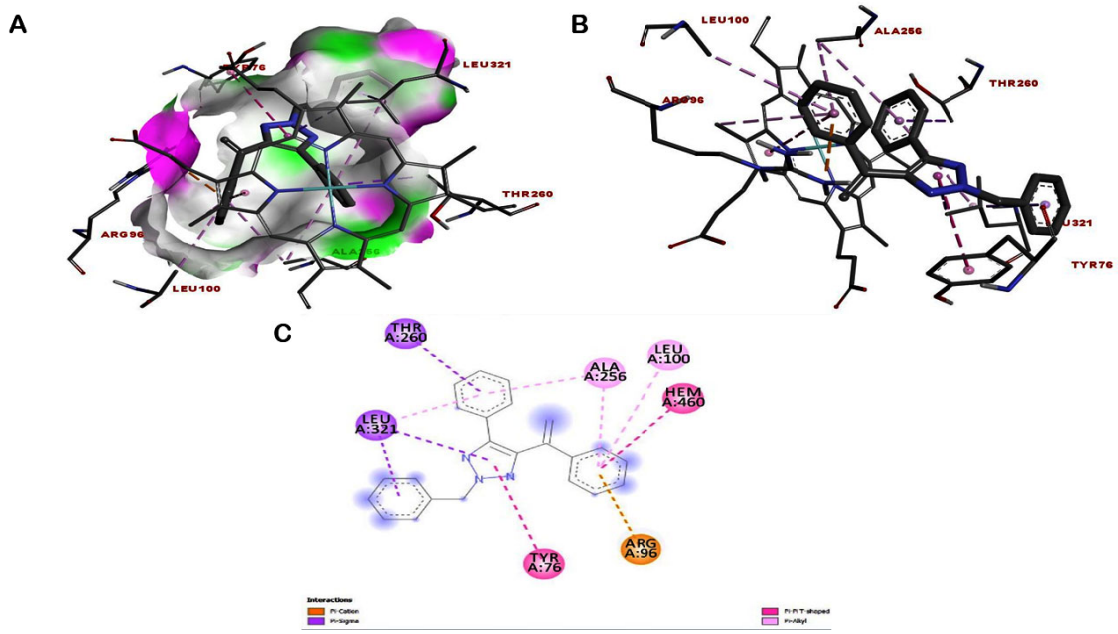

Fig. 4 — Best docking results (CID-139251519, -10.6 kcal/mol) against the cytochrome P450 (CYP51) (PDB ID: 1EA1) from Mycobacterium source. (A) The ligand molecule (black stick) was docked inside the binding pocket of the target protein. Protein residues around the ligand are shown as sticks with residue names and sequence numbers labeled in red. A molecular surface (semi-transparent white/gray) indicates the protein's surface around the ligand. Color shading (green and magenta), highlighting specific surface properties or interaction regions, where green color represents the hydrophobic regions, and the magenta indicates the aromatic or π–π interaction areas. The dashed lines show potential interactions (*e.g.*, hydrogen bonds, π–π stacking, *etc.*); (B) The amino acid residues of the target protein are specifically labeled with residue names, chain identifiers, and positions; and (C) The most important interactions between the ligand and the target protein are shown. The types of interactions are shown in different color codes on the left and right sides

carbon atoms present in the ligand ring structures, whereas Arg96 showed Pi-cation interaction.

The other ligand (CID-101187610; -10.5 kcal/mol) with the best interactions showed interactions with Phe78, Val434, Leu321, Ala256, and Leu100 (Pi-Pi bond formation). The Gln72 and Arg96 displayed hydrogen bond formation with the ligand (Table 1).

Docking against fungal CYP51 target

Sterol biosynthesis is an important part of lipid metabolism in any organism. CYP51 (sterol 14α-demethylase), a member of the cytochrome P450 (CYP) superfamily, is an important protein for sterol biosynthesis and a validated target for antifungal compounds[40]. The CYP51 protein from *Candida glabrata* origin was considered to evaluate the selected molecules (n=173). The ligands, CID-59814079 and CID-59814075, showed the best affinity towards the fungal target protein with a binding energy of -13.8 kcal/mol and -13.7 kcal/mol, respectively (Fig. 5A & B, and Table 1). Analysis of the molecular interactions suggested that CID-59814079 showed interactions with the Ile140, Tyr141, Phe242, Leu381, Met512, His382, and Tyr73 residues. Most of these interactions were various Pi-Pi interactions, except Met512, which formed hydrogen bonding with the compound (Fig. 5C). The compound CID-59814075 showed interactions with Leu96, Tyr73, Ile140, Tyr141, Met512, Phe242, and Leu81 of the target protein.

Analyses of the higher binding energy-containing compounds against the four selected targets showed that CID-135064814, CID-102473643, CID-135066341, CID-135065731, CID-59814079, CID-21331374, CID-88817443, CID-59814075, CID-54036863, and CID-70598857 were the most potent small molecules that could be considered to have antibacterial, antifungal, antidiabetic, and anticancer properties simultaneously, while considering these target proteins. Analysis of the best-docked moleculesThe top four molecules, *i.e.*, CID-135064814 for antidiabetic/anticancer HDAC8 protein, CID-59814079 for anticancer APC protein, CID-139251519 for anti-Mycobacterium CYP protein, and CID-59814079 for antifungal CYP51

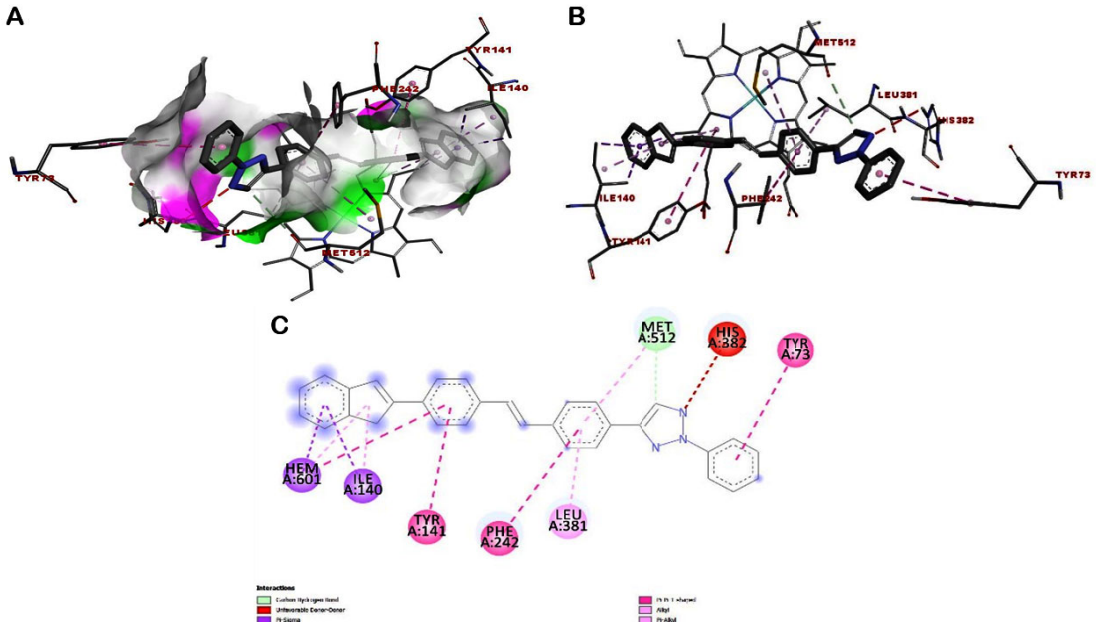

Fig. 5 — Best docking results obtained (CID-59814079; binding energy -13.8 kcal/mol) for the antifungal target protein CYP51 from Candida glabrata (PDB ID: 5JLC). (A) The ligand molecule (black stick) was docked inside the binding pocket of the target protein. Protein residues around the ligand are shown as sticks with residue names and sequence numbers labeled in red. A molecular surface (semi-transparent white/gray) indicates the protein's surface around the ligand. Color shading (green and magenta), highlighting specific surface properties or interaction regions, where green color represents the hydrophobic regions, and the magenta indicates the aromatic or π–π interaction areas. The dashed lines show potential interactions (*e.g.*, hydrogen bonds, π–π stacking, *etc.*); (B) The amino acid residues of the target protein are specifically labeled with residue names, chain identifiers, and positions; and (C) The most important interactions between the ligand and the target protein are shown. The types of interactions are shown in different color codes on the left and right sides

protein were subjected to further analysis to understand their plausible targets in the human proteome as shown for the top 50 hits (Fig. 6). The analysis suggested that CID-135064814 predominantly had targeting affinity for the AG protein-coupled receptor family (28%) (Fig.6A), CID-59814079 also had targeting affinity for the AGprotein-coupled receptor family (34%), followed by kinase proteins (28%) (Fig. 6B & D). CID-139251519 showed target affinity for the same AG protein-coupled receptor family (30%) (Fig. 6C).

We considered performing molecular dynamics (MD) simulations of the best-docked molecule in this study, *i.e.*, CID-59814079, with a binding energy of -13.8 kcal/mol against the antifungal target protein CYP51 from *Candida glabrata (*PDB ID: 5JLC).

Molecular dynamics simulation

RMSD of protein

The protein Root Mean Square Deviation (RMSD) plot (Fig. 7A) demonstrated structural conformational changes of the protein following ligand binding, as seen by the initial rise in RMSD from approximately 0.1 nm to around 0.4-0.5 nm within the first 20 ns. This increase indicated structural modifications in the binding site to facilitate ligand binding.After the equilibration phase, the RMSD stabilized at ~0.3 nm and exhibited slight fluctuations for the rest of the simulation, signifying that the protein-ligand complex attains and sustains a stable shape. The observed transient peaks, such as ~60 ns, may indicate localized or transient flexibility, which could be crucial for ligand stabilization or protein functionality. The ligand seems to stabilize the protein without inducing structural destabilization, facilitating a balance between overall stability and localized flexibility, both essential for biological function.

RMSD of ligand

The ligand Root Mean Square Deviation (RMSD) plot (Fig. 7B) of the ligand during the 100 ns simulation offers insights into its stability and conformational dynamics inside the binding site. Initially, the RMSD increases significantly from 0.05 nm to 0.15 nm, indicating the ligand's accommodation within the binding pocket during the

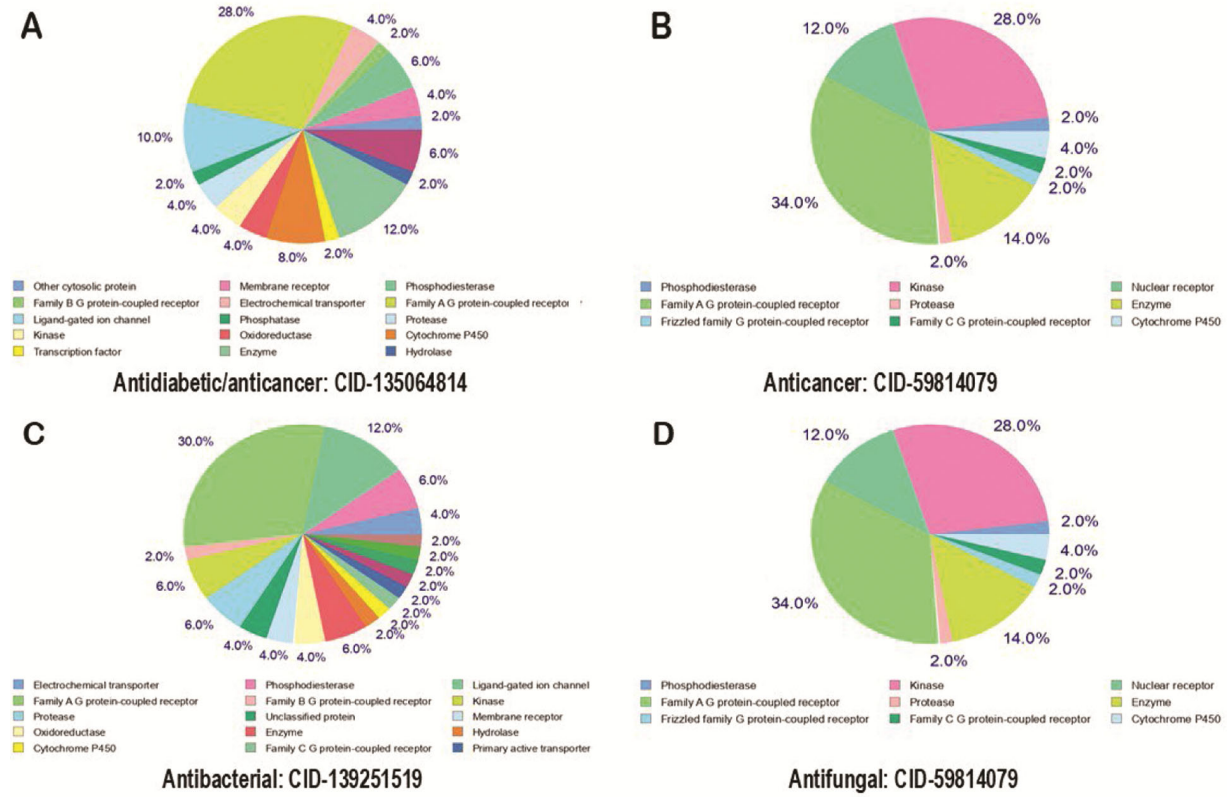

Fig. 6 — The top 50 drug target cellular components predicted for the respective best docking score containing compounds against the selected protein targets. (A) Presentation of the cellular drug targets for the best docked drug molecule (CID-135064814) against the antidiabetic and anticancer protein target; (B) Presentation of the cellular drug targets for the best docked molecule (CID-59814079) against the anticancer protein target; (C) Presentation of the cellular drug targets for the best docked drug molecule (CID-139251519) against the antibacterial protein target; and (D) Presentation of the possible cellular drug targets for the best docked drug molecule (CID-59814079) against the antifungal protein target

equilibration phase. Later, the RMSD stabilized between 0.15 and 0.2 nm. This stabilization signifies that the ligand is effectively positioned within the binding site and preserves a consistent binding conformation with reference to the initial structure. The enhanced RMSD reflected temporary structural flexibility or minor positional modifications; however, they do not signify substantial displacement or instability. The ligand exhibited steady and consistent interactions with the protein, indicating a strong and significant binding within the complex.

Conformation of the ligand

The 3D conformations (Fig. 7B) of the protein-ligand complexes at 0 ns and 100 ns provided significant insights into the structural alterations and stability of the complex throughout the simulation. At the reference conformation (0 ns), the protein's secondary structure and the ligand's binding orientation indicated a well-defined interaction within the binding pocket, influenced by the initial docking. At 100 ns, the protein's overall structure remained predominantly intact, signifying global stability. Subtle modifications in the ligand's binding region and orientation were observed, indicating its adaptation and optimization inside the binding site throughout the simulation. These modifications aligned with the observed stabilization of RMSD following the equilibration phase, as the ligand optimized its binding interactions. The ligand stayed firmly attached within the binding pocket, with localized flexibility enhancing functional dynamism. The comparative study of the two poses (0 ns *vs*. 100 ns) (Fig. 8A) underscores the complex's dynamic stability, confirming the strong binding contact of the ligand with the protein during the simulation.

Interaction analysis

The 2D interaction (Fig. 8A) of the protein-ligand complexes at 0 ns and 100 ns depicted the critical

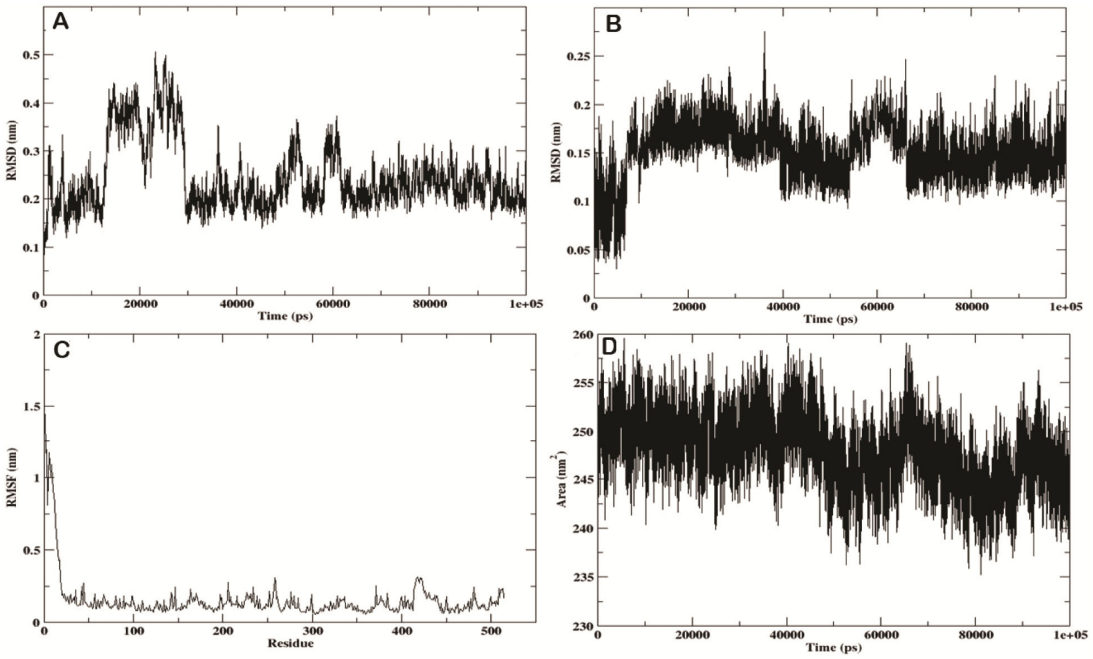

Fig. 7 — (A) RMSD of the Cα atoms of the protein aligned over the initial structure of the complex; (B) RMSD of the ligand for 100 ns MD simulation aligned over the initial structure of the complex; (C) RMSF of the protein residues for the 100 ns MD simulation; and (D) SASA of the protein for the 100 ns MD simulation

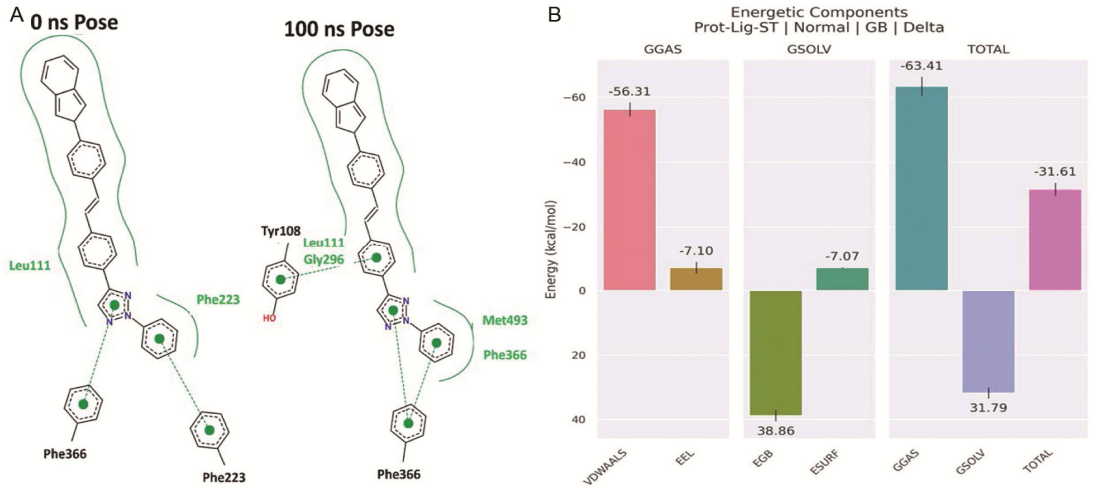

Fig. 8 — (A) 2D representation of the protein-ligand complexes interaction for 0 ns pose and100 ns pose; and (B) The binding free energy of the protein-ligand complex for the last 20 ns MD simulation

interactions throughout the simulation. At 0 ns (Fig. 8A), the ligand engaged with residues including Leu111, Phe223, and Phe366 *via* hydrophobic interactions, supplemented by π-π stacking stabilization. These interactions securely positioned the ligand within the binding pocket, establishing a stable initial conformation. At 100 ns (Fig. 8A), new interactions have been identified, including Tyr108, Met493, and Gly296, whereas interactions with Leu111 and Phe366 were maintained. These modifications indicated that the ligand changed its binding conformation to maximize interactions during the simulation, thus improving stability. The continuity of essential residues such as Leu111 and Phe366 throughout the simulation highlights their vital function in sustaining ligand binding. The dynamic but stable binding interactions aligned with the RMSD trend, strengthening the conclusion that the protein-ligand complex attained a well-adapted and stable conformation by the completion of the simulation.

RMSF of the protein

The Root Mean Square Fluctuation (RMSF) plot (Fig. 7C) of the protein residues throughout the 100 ns simulation offered comprehensive insights into the flexibility of the protein structure. The RMSF quantified the average positional deviations of each residue with reference to the protein's mean conformation, aiding in the identification of flexible areas and residues essential for stability. The residues adjacent to the N-terminus displayed elevated RMSF values (>1.5 nm), signifying considerable flexibility. This was prevalent in terminal locations due to their frequent exposure and reduced structural constraints. After the initial residues, the RMSF stabilizes to lower values (0.1-0.5 nm) across most of the protein, suggesting that the core structure remained relatively rigid and stable throughout the simulation. Localized flexibility was indicated by maxima in RMSF at specific residue indices such as the loops, solvent-exposed areas, or domains engaged in dynamic interactions with the ligand or other molecules. The generally low RMSF values for most residues indicated the protein's structural stability throughout the simulation.

SASA of the protein

The Solvent Accessible Surface Area (SASA) plot (Fig. 7D) of the protein during the 100 ns molecular dynamics simulation elucidated the protein's solvent exposure and structural dynamics. The SASA varied between ~230 nm² and ~260 nm², reflecting dynamic modifications in the protein's surface area during interactions with the surrounding environment. The continuous fluctuations noted during the simulation indicated that the protein preserves a stable overall structure while experiencing temporary alterations in solvent exposure. These alterations may relate to localized conformational adjustments, such as shifts in loop regions, side chains, or flexible residues, rather than extensive unfolding or destabilization. Observed transient fluctuations in SASA may indicate particular interactions between the protein and the ligand, as binding or conformational alterations in the binding pocket could modify the exposure of hydrophobic or hydrophilic areas to the solvent. The SASA analysis confirmed the protein's structural stability during the simulation, while also revealing localized and transitory dynamics in solvent exposure, associated with functional flexibility and ligand interactions.

Binding free energy assessment

The analysis of binding free energy (Fig. 8B) for the protein-ligand complex during the final 20 ns of the MD simulation indicated that van der Waals interactions were the predominant factors in binding stability, exhibiting a substantial energy of -56.31 kcal/mol, underscoring the significance of hydrophobic and dispersion forces. Electrostatic interactions were -7.10 kcal/mol, indicating a secondary role in stabilizing the complex. The solvation energy presented an adverse polar component (38.86 kcal/mol) attributed to desolvation expenses, partially counterbalanced by the favorable nonpolar solvation energy (-7.07 kcal/mol). The overall gas-phase energy (-63.41 kcal/mol) significantly stabilized the complex, whereas the solvation energy (31.79 kcal/mol) marginally counteracted binding. The total binding free energy of -31.61 kcal/mol signifies a favorable and persistent association, underscoring the significance of hydrophobic interactions in the binding pocket, and secondary electrostatic and solvation effects.

Discussion

Among successful synthetic compound generation that is not available naturally, 1,2,3-triazole scaffolds are the important ones due to their widespread applications as antimicrobial, anticancer, antidiabetic, and antiviral usage[41-42]. These compounds are being used with high therapeutic reliability. The structural benefit of the presence of the nitrogen-bearing heterocyclic scaffold allows a synthetic chemist to develop multiple and diverse derivatives of the compounds using reliable and acceptable green chemistry approaches. Moreover, using different metal catalysts is easier for the synthesis of these groups of molecules. Triazoles are considered bioisosteres due to the presence of similar and equivalent physical and chemical properties among the vast number of generated molecules. The reports available in the literature suggest that these compounds are used for various pathogenic conditions, and different FDA-approved drugs are also available in the market[43]. Numerous reports have suggested the effectiveness of these compounds against specific bacteria, such as ESKAPE pathogens[44], as anticancer compounds for colorectal cancer[35], antidiabetic[25], antifungal[23], and others.

The therapeutic efficacy against various pathogens and the opportunity for novel compound development applying reactions related to alkynes, NaN3, alkyl halides, and aryl halides under optimized and appropriate conditions attracted global researchers to

develop more compounds in these series and compare their pharmacological properties with the existing molecules, aiding in replenishing the available drug molecules in the drug discovery pipeline and may help in addressing multi-drug resistance (MDR).

Individually, these compounds have been screened, targeted, and evaluated against particular pathogens or target proteins. However, collective analyses or assessments of the potential of these compounds against multiple targets are limited. In this study, we screened 173 molecules using the drug screening filters in the PubChem database and evaluated those molecules against multiple target proteins to screen molecules that may have equivalent therapeutic potential for antidiabetic, anticancer, antibacterial, and antifungal treatment.

Certain compounds (CID-135064814, CID-102473643, CID-135066341, CID-135065731, CID-59814079, CID-21331374, CID-88817443, CID-59814075, CID-54036863, and CID-70598857) showed excellent binding affinity towards the selected target proteins. This was achieved due to the microenvironment and the distribution of the amino acids in the pocket regions of the selected target proteins, and the respective pocket volumes, size, and shape also supported the best interactions.

The ADMET properties of these compounds were acceptable in most cases, ideal for considering them as therapeutic molecules. The docking scores obtained in each case suggested strong binding affinity, and the molecular dynamics simulation done for the antifungal target showed excellent binding dynamics and interactions of the selected compound. This is one of the few studies in which we have attempted to screen and sort multiple triazole compounds that may be effective against multiple targets simultaneously.

However, further consideration should be there to considering more target proteins and molecules simultaneously, along with possible inclusion of QSAR, extended MD simulations, followed by experimental evaluations.

Conclusion

This study was an attempt to screen multiple triazole compounds that could be used as a potential therapeutic agent for multiple conditions, such as diabetes and cancer, and against different pathogens, such as bacteria and fungi, simultaneously. We employed molecular modelling approaches such as docking, MD simulation, and associated computational approaches to screen the molecules against the considered targets and were able to identify the compounds that may have the potential to become therapeutic agents against these targets.

Acknowledgement

The authors are thankful for the management and staff of GITAM School of Pharmacy, GITAM (Deemed to be) University, Hyderabad and Sarojini Naidu Vanita Pharmacy Maha Vidyalaya, Secunderabad, for their constant support and encouragement.

Conflict of interest

All authors declare no conflict of interest.

References

1 Ueda S, Su M & Buchwald S, Highly N2-Selective Palladium-Catalyzed Arylation of 1,2,3-Triazoles. *Angewandte Chemie Int Ed*, 50 (2011) 8944.

2 Baidya M, Mallick S & Sarkar SD, Regioselective Synthesis of N 2-Aryl 1,2,3-Triazoles *via* Electro-oxidative Coupling of Enamines and Aryldiazonium Salts. *Org Lett*, 24 (2022) 1274.

3 RoshandelS, Lunn MJ, Rasul G, Ravinson DSM, Suri SC & Prakash GS, Catalyst-Free Regioselective N2 Arylation of 1,2,3-Triazoles Using Diaryl Iodonium Salts. *Org Lett*, 21 (2019) 6255.

4 Li J, He Y, Wang L, Pan Q, Song Z & Shi X, Design and synthesis of photoluminescent active interpenetrating metal–organic frameworks using N-2-aryl-1,2,3-triazole ligands. *Dalton Trans*, 49 (2020) 5429.

5 Arora N & Banerjee AK, Computer-Aided Drug Design for Combating Diseases (Part-IV). *Curr Top Med Chem*, 21 (2021) 2243.

6 Dahiya P, Banerjee A, Saha A, Nandicoori VK, Ghosh S & Mukhopadhyay S, Structure-function relationship of PE11 esterase of Mycobacterium tuberculosis with respect to its role in virulence. *Biochem Biophys Res Commun*, 739 (2024) 150927.

7 Bibi S & Sakata K, Current status of computer-aided drug design for type 2 diabetes. *Curr Comput-Aided Drug Des*, 12 (2016) 167.

8 Rashdan HR, Abdelmonsef AH, Abou-Krisha MM & Yousef TA, Synthesis, identification, computer-aided docking studies, and ADMET prediction of novel benzimidazo-1,2,3-triazole based molecules as potential antimicrobial agents. *Molecules*, 26 (2021) 7119.

9 O'Boyle NM, Banck M, James CA, Morley C, Vandermeersch T & Hutchison GR, Open Babel: An open chemical toolbox. *J Cheminformatics*, 3 (2011) 1.

10 Bento AP, Hersey A, Félix E, Landrum G, Gaulton A, Atkinson F, Bellis LJ, De Veij M & Leach AR, Anopen source chemical structure curation pipeline using RDKit. *J Cheminformatics*, 12 (2020) 1.

11 Daina A, Michielin O & Zoete V, SwissADME: a free web tool to evaluate pharmacokinetics, drug-likeness and medicinal chemistry friendliness of small molecules. *Sci Rep*, 7 (2017) 42717.

12 Huey R, Morris GM & Forli S, Using AutoDock 4 and AutoDockvina with AutoDockTools: a tutorial. The Scripps

Research Institute Molecular Graphics Laboratory. 10550 (2012) 1000.
13 Visualizer DS, Discovery Studio Visualizer. 2. Accelrys software inc. 2005.
14 Huang J & MacKerell Jr AD, CHARMM36 all-atom additive protein force field: Validation based on comparison to NMR data. *J Comput Chem*, 34 (2013) 2135.
15 Bauer P, Hess B & Lindahl E, GROMACS 2022.4 Manual (2022.4). Zenodo. 2022; 3: 190.
16 Vanommeslaeghe K, Hatcher E, Acharya C, Kundu S, Zhong S, Shim J, Darian E, Guvench O, Lopes P, Vorobyov I & Mackerell Jr AD, CHARMM general force field: A force field for drug-like molecules compatible with the CHARMM all-atom additive biological force fields. *J Comput Chem*, 31 (2010) 671.
17 Darden T, York D & Pedersen L, Particle mesh Ewald: An N· log (N) method for Ewald sums in large systems. *J ChemPhys*, 98 (1993) 10089.
18 Harrach MF & Drossel B, Structure and dynamics of TIP3P, TIP4P, and TIP5P water near smooth and atomistic walls of different hydroaffinity. *J Chem Phys*, 140 (2014) 174501.
19 Hess B, Bekker H, Berendsen HJ & Fraaije JG, LINCS: a linear constraint solver for molecular simulations. *J Comput Chem*, 18 (1997) 1463.
20 Bussi G, Donadio D & Parrinello M, Canonical sampling through velocity rescaling. *J Chem Phys*, 126 (2007) 014101.
21 Martoňák R, Laio A & Parrinello M, Predicting crystal structures: the Parrinello-Rahman method revisited. *Phys Rev Lett*, 90 (2003) 075503.
22 Strzelecka M & Świątek P, 1, 2, 4-Triazoles as important antibacterial agents. *Pharmaceuticals*, 14 (2021) 224.
23 Kazeminejad Z, Marzi M, Shiroudi A, Kouhpayeh SA, Farjam M & Zarenezhad E, Novel 1, 2, 4-Triazoles as Antifungal Agents. *BioMed Res Int*, 2022 (2022) 4584846.
24 Hu Y, Liu Z, Zha G, Long S, Sridhara MB, Kumar KS & Rakesh KP, Triazole derivatives as potential antifungal agents: A structure-activity relationship (SAR) studies. *Process Biochem*, 135 (2023) 102.
25 Fallah Z, Tajbakhsh M, Alikhani M, Larijani B, Faramarzi MA, Hamedifar H, Mohammadi-Khanaposhtani M & Mahdavi M, A review on synthesis, mechanism of action, and structure-activity relationships of 1,2,3-triazole-based α-glucosidase inhibitors as promising anti-diabetic agents. *J Mol Struct*, 1255 (2022) 132469.
26 Sharma A, Dubey R, Bhupal R, Patel P, Verma SK, Kaya S & Asati V, An insight on medicinal attributes of 1,2,3-and 1, 2, 4-triazole derivatives as alpha-amylase and alpha-glucosidase inhibitors. *Mol Divers*, 28 (2023) 3605.
27 Alam MM, 1,2,3-Triazole hybrids as anticancer agents: A review. *Archiv der Pharmazie*, 355 (2022) 2100158.
28 Bhagat DS, Bumbrah GS, Chawla PA, Gurnule WB & Shejul SK, Recent advances in synthesis and anticancer potential of triazole-containing scaffolds. *Anticancer Agents Med Chem*, 22 (2022) 2852.
29 Sharma A, Agrahari AK, Rajkhowa S & Tiwari VK, Emerging impact of triazoles as anti-tubercular agent. *Eur J Med Chem*, 238 (2022) 114454.
30 ErazuaEA, Akintelu SA, Adelowo JM, Odoemene SN, Josiah OM, Raheem SF, Latona DF, Adeoye MD, Esan AO & Oyebamiji AK, QSAR and molecular docking studies on nitro (triazole/imidazole)-based compounds as anti-tubercular agents. *Trop J Nat Prod Res*, 5 (2021) 2022.
31 Wang L, Bai Y, Cao Z, Guo Z, Lian Y, Liu P, Zeng Y, Lyu W & Chen Q, Histone deacetylases and inhibitors in diabetes mellitus and its complications. *Biomed Pharmacother*, 177 (2024) 117010.
32 Chakrabarti A, Oehme I, Witt O, Oliveira G, Sippl W, Romier C, Pierce RJ & Jung M, HDAC8: a multifaceted target for therapeutic interventions. *Trends Pharmacol Sci*, 36 (2015) 481.
33 Shafique K, Farrukh A, Mahmood Ali T, Qasim S, Jafri L, Abd-Rabboh HS, Al-Anazy MM & Kalsoom S, Designing Click One-Pot Synthesis and Antidiabetic Studies of 1,2,3-Triazole Derivatives. *Molecules*, 28 (2023) 3104.
34 Hankey W, Frankel WL & Groden J, Functions of the APC tumor suppressor protein dependent and independent of canonical WNT signaling: implications for therapeutic targeting. *Cancer Metastasis Rev*, 37 (2018) 159.
35 Zhang L & Shay JW, Multiple roles of APC and its therapeutic implications in colorectal cancer. *J Natl Cancer Inst*, 109 (2017) djw332.
36 Zhang Z, Chen L, Gao L, Lin K, Zhu L, Lu Y, Shi X, Gao Y, Zhou J, Xu P & Zhang J, Structural basis for the recognition of Asef by *Adenomatous Polyposis* coli. *Cell Res*, 22 (2012) 372.
37 Podust LM, Poulos TL & Waterman MR, Crystal structure of cytochrome P450 14α-sterol demethylase (CYP51) from *Mycobacterium tuberculosis* in complex with azole inhibitors. *Proc Natl Acad Sci U S A*, 98 (2001) 3068.
38 Keniya MV, Sabherwal M, Wilson RK, Woods MA, Sagatova AA, Tyndall JD & Monk BC, Crystal structures of full-length lanosterol 14α-demethylases of prominent fungal pathogens Candida albicans and Candida glabrata provide tools for antifungal discovery. *Antimicrob Agents Chemother*, 62 (2018) 10.
39 Jendele L, Krivak R, Skoda P, Novotny M & Hoksza D, PrankWeb: a web server for ligand binding site prediction and visualization. *Nucleic Acids Res*, 47 (2019) W345.
40 Hargrove TY, Kim K, Soeiro MD, da Silva CF, Batista DD, Batista MM, Yazlovitskaya EM, Waterman MR, Sulikowski GA & Lepesheva GI, CYP51 structures and structure-based development of novel, pathogen-specific inhibitory scaffolds. *Int J Parasitol Drugs Drug Resist*, 2 (2012) 178.
41 Vala DP, Vala RM & Patel HM, Versatile synthetic platform for 1,2,3-triazole chemistry. *ACS Omega*, 7 (2022) 36945.
42 Sunkara MS, Tangeda SJ, Annepally D, Bıtla D K, Boppy S, Chidurala P & Chıluka J, Targetting the 3BGQ-PIM1 kinase interaction with a series of novel dithiocarbamate substituted 2-oxoindole derivatives-*in silico* studies. *J Facult Pharm Ankara Univer,* 1 (2022) 46.
43 Vaishnani MJ, Bijani S, Rahamathulla M, Baldaniya L, Jain V, Thajudeen KY, Ahmed MM, Farhana SA & Pasha I, Biological importance and synthesis of 1,2,3-triazole derivatives: a review. *Green Chem Lett Rev*, 17 (2024) 2307989.
44 Sunkara MS & Beda DB, Design, synthesis, and antidiabetic evaluation of N-2-aryl-1,2,3-triazoles (NATs) as potent α-amylase and α-glucosidase inhibitors: a computational and biochemical investigation. *J Mol Struct*, 1343 (2025) 142771.